J Ther Eng, Vol. 10, No. 4, pp. 868−879, July, 2024

Journal of Thermal Engineering
Web page info: https://jten.yildiz.edu.tr
DOI: 10.14744/thermal.0000846

Research Article

Thermo-fluid performance of a heat exchanger with a novel perforated flow deflector type conical baffles

Md. Atiqur RAHMAN[1,*], Sushil Kumar DHIMAN[2]

[1]Department of Mechanical Engineering, Vignan's Foundation for Science, Technology & Research (Deemed to be University), Vadlamudi, Guntur, Andhra Pradesh, 522213, India
[2]Department of Mechanical Engineering, Birla Institute of Technology, Mesra, Ranchi, Jharkhand 835215, India

ARTICLE INFO

Article history
Received: 16 May 2023
Revised: 27 July 2023
Accepted: 30 August 2023

Keywords:
Conical Baffle Plate; Inclination Angle; Rectangular Deflector; Swirl Flow; Thermal Efficiency; Volume Goodness Factor

ABSTRACT

A study investigated how a new swirl airflow design could impact the heat transfer rate in a tubular heat exchanger with axial flow. A perforated conical baffle plate with rectangular air deflectors of different inclination angles was created to generate a swirl flow. The tubes in the heat exchanger were aligned longitudinally, and the heat flux across their surface was kept constant. Each plate had four deflectors with equal deflector angles and adjustable pitch ratios, which created a swirling airflow inside the circular duct containing the heated tubes. This increased turbulence and the rate of heat transfer across the tube surface. The Reynolds number stayed within the range of 93,500 to 160,500. The result indicates that the inclination angle and Pitch ratio profoundly impact the Nusselt number, while the pitch ratio has a greater effect on the friction factor. Furthermore, the conical baffle plate design resulted in an average improvement of 2.51 in thermal efficiency compared to a segmental baffle design with a deflector angle of 30° and a pitch ratio of 1, all under similar Reynolds number, pitch ratio, and blockage ratio conditions.

Cite this article as: Rahman MA, Dhiman SK. Thermo-fluid performance of a heat exchanger with a novel perforated flow deflector type conical baffles. J Ther Eng 2024;10(4):868−879.

INTRODUCTION

Researchers have been drawn to creating small, effective heat exchangers due to the demands of modernization and global energy needs. These heat exchangers, known as HXs, are widely used and have been the subject of ongoing research to improve their ability to transfer heat. Enhancing HT can be achieved through active, passive, or compound methods, all aimed at reducing the resistance to heat flow on a heated surface [1]. However, these methods increase heat transfer and result in higher pressure drops, necessitating more pumping power.

There are two distinct methods of heat augmentation technique; one that requires a supplementary external power source must be employed to enhance the heat transfer rate, which can be either incorporated into the heated surface or the fluids, based on the system needs [2,3]. The second method is the passive method, where augmentation in heat transfer rate is accomplished by either surface

***Corresponding author.**
*E-mail address: rahman.md4u@gmail.com

This paper was recommended for publication in revised form by Editor-in-Chief Ahmet Selim Dalkılıç

Published by Yıldız Technical University Press, İstanbul, Turkey

modification, such as extended surface, to produce turbulence in the flow, thus upsetting the thermal boundary layer. There has been a rise in the implementation of passive techniques in recent times. These techniques, including artificial roughness, extended surface/mesh inserts [4,5], swirl devices, and vortex generators, aim to enhance fluid mixing and minimize or eliminate the thermal boundary layer. Swirl devices, in particular, have gained popularity in increasing h_m by inducing an additional vortex flow that diminishes the thickness of the boundary layer [6]. Recently, several studies have investigated various devices utilizing swirl flow, such as conical rings, twisted tape, and helical wire [7]. Swirl flow has proven to be applicable in several areas including heat exchangers [8], bubble generators [9], cyclone separators [10,11,12], pumps [13,14], and the cooling of electronic components using nanoparticles [15-19].

Swirl flow is characterized by a helical or spiral flow path, as depicted in Figure 1. It occurs when fluid particles possess both axial and tangential components of velocity, resulting in a rotational movement along an axis. If the flow is given through some confined path such as a shell either by suction or/and by forced flow generating device, the flow is a helical swirl while the device may be an axial flow fan or a propeller.

Swirling motion can be achieved in an HX by geometrical retrofitting. The retrofitting is generally made with baffles that support the tubes in an STHX [20,21]. Baffles also facilitate the flow redirection and manage the purposeful transmission of fluid (gas or liquid) through the heat exchanger. The heat exchange occurs between the fluids on the shell side and tube side depending on the relative hotness of either fluid towards the cold one. Many geometrical variables like shell length, shell diameter, tube length, baffle spacing, and baffle cutting space are significant features directly related to heat transfer success. To maintain the fluid flow pattern (parallel counter or cross flow) and to support the tube bundles, a different configuration of the baffles plays a vibrant role in improving both Δp and HT performance [22]; thus, tube bundles and baffles configurations have a dominant role in HX performance [23-25]. Numerous single and double baffle designs have been researched for single baffle; a baffle cut of 20-25% and 40-45% for liquid and gas, respectively, are preferred [26,27].

Swirl motion inside a duct can also be achieved using turbulators; a few relevant works are discussed below.

Kongkaitpaiboon et al. [28,29] conducted various experiments on the use of conical rings (perforated) with different pitch ratios (4 - 12) and several perforation hole numbers (4 - 8) in the heat exchanger (HX) system. They observed a significant increase in HT compared to a smooth pipe, with a 137% higher heat transmission rate. The circular ring turbulator proved most effective in heat transfer when operated within a Reynolds number range of 4000-23000. The researchers found lower diameter and pitch ratio values yielded the best heat transfer performance.

Rahman and Dhiman [30,31] conducted studies on perforated baffle plates, revealing that a duct with these plates demonstrated significantly better thermo-fluid performance than a duct without them. Specifically, in the range of *Re* from 16000 to 28000, the duct with perforated flow deflector baffle plates achieved an average of 3.75 times higher performance with a deflector with α of 50° and *PR* of 1.4. Additionally, when the flow orientation changed from parallel to counter flow, there was an average 7.4% improvement in PEC when the deflector with α was set to 30°, with the highest HX effectiveness observed at lower α and high *PR* values. Rahman [32,33] further examines the effect of rectangular perforation with one and two flow deflectors for each perforation. The effect of deflector orientation on HT and f was experimentally determined. In the case of one flow deflector, the Nu showed 41.49% augmentation in thermal-fluidic performance(R). In contrast, using two flow deflectors with opposite orientations was observed 0.19 times in the TEF compared to HX with a segmental baffle plate. The result demonstrates a higher heat transfer rate in opposite-oriented deflectors than inline ones, and the advantage comes with higher frictional losses.

The literature deliberated numerous methods of passive enhancement of HT. The best optimistic practice is swirling flows; a few standard swirl producers are discoursed: conical ring, twisted tape, and helical coil. An unconventional swirl-producing design applicable to the HX application has been discussed [30-33], a form of perforation with a flow deflector for a flat baffle plate. This investigation explores the possibility of the implication of the techniques mentioned (Perforation with flow deflector) above on a conical baffle plate. Additionally, research involving air as working fluids is limited in the mentioned texts.

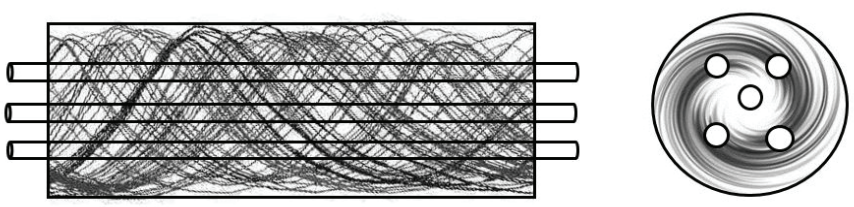

Figure 1. Swirl motion in a heat exchanger.

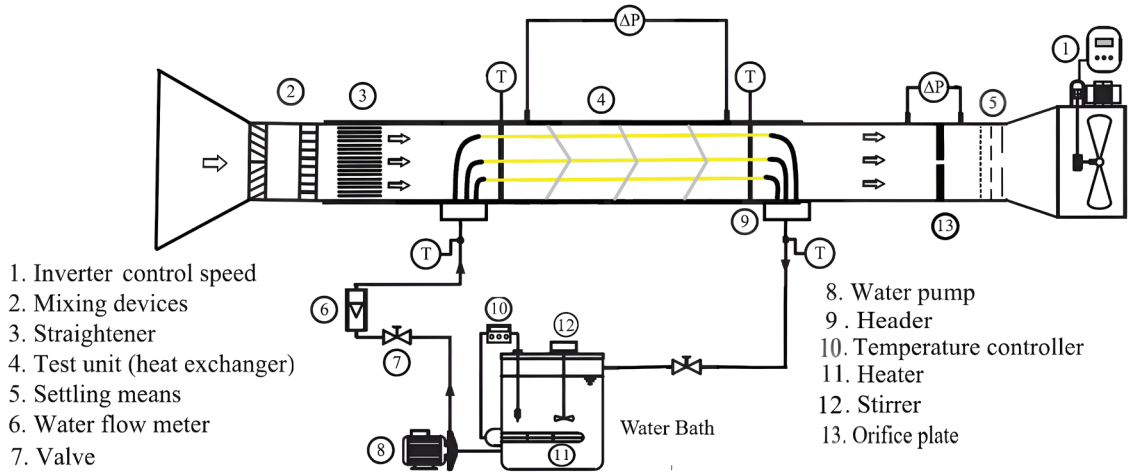

Figure 2. The experimental setup's schematic [From Rahman and Dhiman [30]].

This research focuses on developing and experimenting with a new baffle plate design that generates swirl motion and turbulence in a flow. The rectangular deflector attached to each baffle plate, located at a distance of 1.5d (12mm) from the center, modifies the path lines to create swirl motion. The plate is positioned at the test section's beginning, resulting in a gradual decrease in swirl intensity downstream. The disruption in the flow increases residence time in the channel and enhances HT. The examination was piloted in a circular acrylic duct and observed the impact of pitch ratio (PR) and inclination angle (α) on HT and *f*. The PR varies between 0.6 - 1.2, while the α ranges between 30° - 50°. The tests are conducted in a consistent inlet arrangement with *Re* range of 93,500 - 160,500. The outcomes are compared between ducts equipped with conical deflector baffle plates (CDBP) and those with standard baffle plates (SBP) at matching PR, BR, and *Re* values. The aim is to monitor the superior performance of baffles with flow deflector.

METHODOLOGY

Experimental Arrangement

Figure 2 illustrates the experimental setup, comprising various components such as a straightener, an axial flow fan, a mixing device, a heat exchanger (HX), an orifice plate, pressure transducers, thermocouple probes, and a DAC. The fan draws ambient air from the surroundings, which is then directed through the air duct. Before entering the HX, the air passes through the mixer and the straightener. Temperature probes, specifically T-type copper-constantan thermocouples, are positioned at the HX's inlet ($T_{a,\ in}$) and outlet ($T_{a,\ out}$) sections to measure air temperature.

Orifice plates are utilized to acquire the airflow rate, rendering ISO5801 standard. Pressure transducers are installed at three locations on both the inlet and exit sides, positioned at a 120° angle from the center of the baffle plate. The pressure drop is measured using a VDAS DAQ card and a differential transducer ranging from 0 to 1 psi with a LabVIEW-assisted data recorder. The water used in the experiment is electrically heated to 60 °C by an 8 kW heater regulated using the thermostat.

Mechanical mixers maintain consistent liquid characteristics (density and temperature) within the bathtub. The flow rate of hot liquid is controlled using a 0.25 hp feed pump, a flow-regulating valve, and a flow-measuring device. The hot liquid is continuously supplied at a rate of 4 LPM into a header, evenly distributed to a network of tubes within the heat exchanger. The positioning of the tubes within the HX and the arrangement of baffles can be found in the subsequent paragraph.

For temperature measurements of the heated water-carrying pipes at different places in the experimental setup, PT100 RTDs are utilized. The experiment maintains a constant hot water flow rate at a specified inlet temperature while adjusting the air circulation flow rate. Before data recording, the system can reach a steady state. After the HX is fully stabilized, the incoming and outgoing air and the surface temperature of the copper tubing are logged. The precision of the immediate measuring device is evaluated using the root mean sum square, with the testing conditions depicted in Table 1. Table 2 provides information about the precision of the measuring instrument, and the associated uncertainties [34] are estimated using equations 1-5 outlined in Table 3.

Table 1. Testing conditions used in experiments

Temperature at inlet (air)	32.5 ± 0.5°C
Mean velocity (air)	7- 13 m/s
Temperature at inlet (water)	55-60°C
Waterflow rate (mass)	0.06 kg/s

Table 2. Accuracy with measurements [30]

Parameter	**Accuracy**
Parameter	Accuracy
Air temperature-intake, °C	±0.5
Pressure drops, Pa	±0.1
Water temperature-intake, °C	±0.5
Water flow rate, kg/s	±0.006

Table 3. Uncertainties with investigational data

Parameter Max skepticism (%)	
Re	±1.73
Nu_m	±2.35
v	±6
f	±4.22
Q	±5

$$\frac{\Delta Nu}{Nu} = \left[\left(\frac{\Delta h}{h}\right)^2 + \left(\frac{\Delta D_h}{D_h}\right)^2\right]^{0.5} \quad (1)$$

$$\frac{\Delta h}{h} = \left[\left(\frac{\Delta Q_{air}}{Q_{air}}\right)^2 + \left(\frac{\Delta T_f}{T_f}\right)^2 + \left(\frac{\Delta T_p}{T_p}\right)^2\right]^{0.5} \quad (2)$$

$$\frac{\Delta Q_{air}}{Q_{air}} = \left[\left(\frac{\Delta v}{v}\right)^2 + \left(\frac{\Delta T_{in}}{T_{in}}\right)^2 + \left(\frac{\Delta T_{out}}{T_{out}}\right)^2\right]^{0.5} \quad (3)$$

$$\frac{\Delta f}{f} = \left[\Delta\left(\frac{\Delta P}{P}\right)^2 + \left(\frac{\Delta L}{\mathrm{L}}\right)^2 + \left(3\frac{\Delta D_h}{D_h}\right)^2 + \left(2\frac{\Delta Re}{Re}\right)^2\right]^{0.5} \quad (4)$$

$$\frac{\Delta \mathrm{Re}}{\mathrm{Re}} = \left[\left(\frac{\Delta v}{v}\right)^2 + \left(\frac{\Delta D_h}{D_h}\right)^2\right]^{0.5} \quad (5)$$

Test Section Specifics

Presented in Figure 3 is a segment of the system containing Plexiglas with k_p of 0.2. It comprises a 60 cm long component with a D =19 cm and a breadth of 0.5 cm. Along this channel (Plexiglass) are copper tubes, specifically DHP Copper tubes of C12200 material, with k_t of 300, an ID of 8mm, and a thickness of 1mm, have been fitted. The copper pipes transport warm liquid or gas while the surrounding air is passed along the duct. Two sets of thermocouples are utilized to capture surface temperature, each with 5 thermocouples for the respective pipe. These thermocouples, labeled T_{w1}- T_{w5}, capture the temperature at the copper pipes inlets and exit. Additionally, thermocouples labeled $T_{a,in,}$ and $T_{a,out}$ are included in Figure 3 to record the air temperature at both the entrance and exit points of the Plexiglas, providing further analysis.

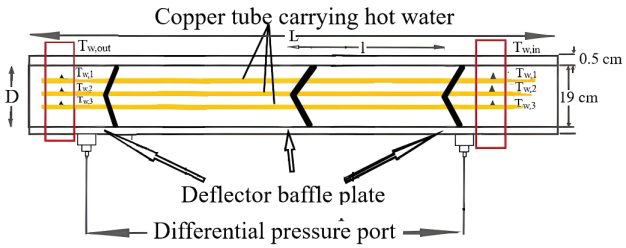

Figure 3. Test section.

Baffle Plate and Tube Organization

The newly printed 3D model, the Conical Deflector Baffle Plate (CDBP), is presented in Figure 4. The CAD representation can be seen in Figure 4a, while the actual investigational model is shown in Figures 4c and 4d. This innovative design features a central tube encircled by four extra tubes organized in a circular pattern. These tubes are spaced 4 cm from the central tube, showing a triangular-pitch formation with a transverse pitch of 8 cm. To facilitate airflow transfer, the CDBP includes four rectangular openings. These perforations size was 7 times the tube diameter (1 cm) to maintain the same blockage ratio as the previous design (SBP), as depicted in Figure 4b.

Four deflectors of the same size as the rectangular perforations (7dxd) were attached at a prearranged angle in contradiction of the baffle plane to shift the airflow from axial to swirl flow, as shown in Figure 4a. This deflector arrangement induces swirling flow amongst the baffle plates, transitioning the airflow into a plug flow pattern when passing through the tube bundles. The angle (α) intensifies the axial flow, leading to plug flow and stimulating swirling streams in the duct. This swirling motion prevents stagnant areas near the baffle and increases pressure, enhancing heat transfer between the baffle plates. The baffle plates' pitch ratio (PR) is crucial as it determines the

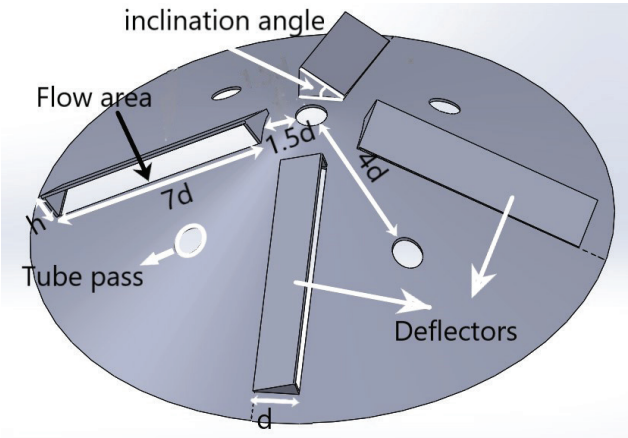

Figure 4a.CAD model of CDBP.

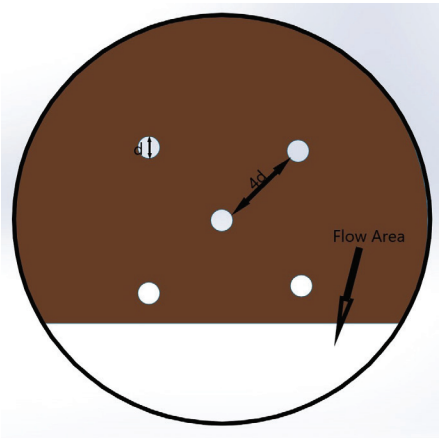

Figure 4b.CAD model of SBP.

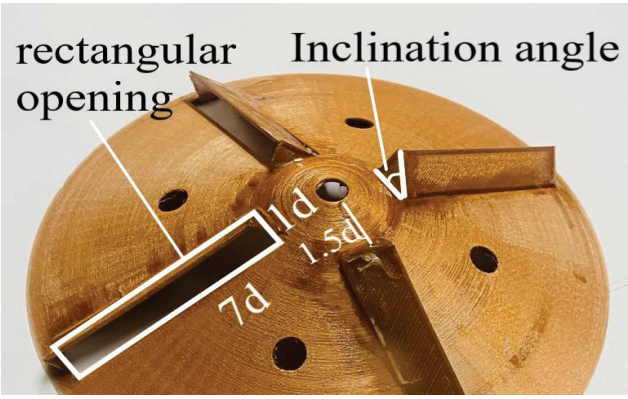

Figure 4c. Pictorial view of conical deflector baffle plat.

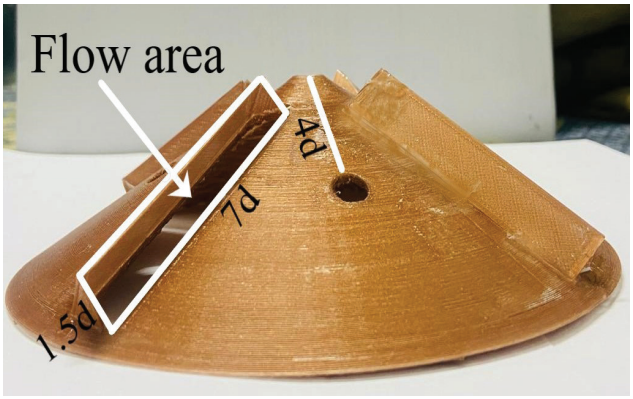

Figure 4d. Design details.

turbulence intensity and recirculation in the channel. The investigation examined PR values of 0.6, 0.8, 1, and 1.2.

Furthermore, air rotation generated turbulence and vortices inside the duct amongst the baffle plates. This continuous movement washes the tube wall and manipulates the thermal boundary layer. The study also considered altered angles (α) of 30°, 40°, and 50°, which influenced the airflow dynamics. The design includes a vent-like component allowing air circulation, creating a flow area. The deflectors are positioned at a distance of 1.5 times the D (10mm) from the epicenter of the Baffle Plate. Additionally, the deflectors possess equal heights (h1=h2), as shown in Figure 4a.

Design Variables Under Study

PR [1, 28, and 32] is estimated as

$$PR = {}^{l}\!/_{D} \tag{6}$$

The blockage ratio [32,33] is estimated using.

$$BR = {}^{E}\!/_{A} \tag{7}$$

E= area of baffle plate cross-sectional - (4 times the area of the opening cross-sectional)

A= area of the baffle plate cross-sectional

This research examined how CDBP flows in a circular pipe with a fixed BR of 0.70. The study looked at different Re values for a longitudinal flow and tested samples with three α: 30°, 40°, and 50°. A duct with SBP at the same BR and similar *Re* ranges was also investigated. The results were analyzed to understand how PR and α affect the thermo fluid performance of the HX. The test section particulars are presented in Table 4.

Table 4. Test section particulars

Duct thickness 0.5 cm
Duct inner diameter (D) 19 cm
Baffle plates used 3
Consecutive baffles plate distance (l) 22.8,19, 15.2, 11.4 cm
Ducts thickness 5 mm
Overall Length of test section (L) 60 cm
Copper tube length 60 cm
Crossectional area of a baffle plate (A) 268.80 cm^2
Baffle plate height 5 cm.

The Cao [35] method is utilized to find h_m.

Below are the listed parameters in question, along with the accompanying equations utilized in their computation:

Re [32,33]:

$$Re = \rho.v.D / \mu \tag{8}$$

The average temperatures of air intake and discharge are utilized to evaluate the thermal characteristics of air, like ρ and μ.

$$v = \sqrt{\frac{2\Delta P}{\rho}} \tag{9}$$

$$h_m = \frac{Q}{A_p \Delta t_{lm}} \tag{10}$$

Q is calculated as [32,33]:

$$Q = C_p \rho v A_c \left(T_{a,out} - T_{a,in}\right) \tag{11}$$

Where $A_c = \frac{\pi}{4}\left(D - D_e\right)$

$T_{a\ in}$, is the air temperature at the inlet, and $T_{a\ out}$ is the temperature of the air leaving the test section.

Δt_{lm} is given as [32,33]:

$$\Delta t_{lm} = \frac{\left(t_{w,in} - t_{a,in}\right) - \left(t_{w,out} - t_{a,out}\right)}{ln\left(t_{w,in} - t_{a,in}\right) / \left(t_{w,out} - t_{a,out}\right)} \tag{12}$$

The tube wall's average temperature at the inlet and $t_{w,\ in,}$ is the tube wall's average temperature, and $t_{w,\ out}$ is the tube wall's average temperature at the exit, respectively. Calculated as [32,33]:

$$T_{w,in} = \left[\frac{\sum_1^5 T_{w,i} A_i}{A_p}\right]_{in}, T_{w,out} = \left[\frac{\sum_1^5 T_{w,i} A_i}{A_p}\right]_{out} \tag{13}$$

One through five are the assigned labels for the thermocouple locations on the wall of copper tube at the test section's entry and departure points, with the designated index "i".

Average value of *Nu*, *j,* and *f* indicates the duct flow's dynamics and heat transfer qualities estimated as [32,33]:

$$Nu = \frac{h_m D}{\lambda} \tag{14}$$

$$j = \frac{Nu}{RePr^{1/3}} \tag{15}$$

$$f = \frac{2\Delta p D}{\rho v^2 L} \tag{16}$$

Δp is the pressure drop in the test section

From Equations 3 and 4

$$h_m = \frac{C_p \rho v A_c (T_{a,out} - T_{a,in})}{A_p \Delta t_{lm}} \tag{17}$$

Thermal efficiency

$$\eta = \left(\frac{Nu}{Nu_s}\right)\left(\frac{f_s}{f}\right)^{1/3} \tag{18}$$

Where Nu_s and f_s are the Nusselt number and friction factor of SBP.

The term Volume goodness factor (VGF=$j/f^{1/3}$) has been introduced [36].

Validation of Experimental Result

Analyses were conducted on the experimental results to assess their accuracy in calculating h_m and *f* for turbulent flows in circular ducts. Specifically, a comparative evaluation was performed, contrasting the experimental findings with the Dittus Boelter and Gnielinski correlation, renowned equations used in this domain.

Nu relationships:

Dittus and Boelter [37] correlation:

$$Nu = 0.023 Re^{4/5} Pr^{0.4} \quad \text{For } Re \geq 1\text{x}10^4 \tag{19}$$

Gnielinski [38] correlation:

$$Nu = \frac{\left(\frac{\xi}{8}\right)\left(Re - 1000\right) Pr}{\left[1 + 12.7\left(\frac{\xi}{8}\right)^{1/2}\left(Pr^{2/3} - 1\right)\right]}\left[1 + \left(\frac{D}{L}\right)^{2/3}\right]\left(\frac{P_{rm}}{P_{rw}}\right)^{0.11} \tag{20}$$

Pr between 0.5-2000 and *Re* between 4000-10^6

Where ξ estimated using the Filonienko correlation:

$$\xi = \left(1.82\ \log\ Re\ - 1.64\right)^{-2} \tag{21}$$

P_{rm} and P_{rw} labeled the *Pr* at the bulk and wall temperature, respectively

f correlation:

Colebrook-White [39] correlation:

$$\frac{1}{\sqrt{f}} = 1.8 \log\left(\frac{Re}{6.9}\right) \quad \text{For } 4000 \leq Re \leq 10^8 \tag{22}$$

Blasius [40]:

$$f = 0.316\ Re^{-0.25} \tag{23}$$

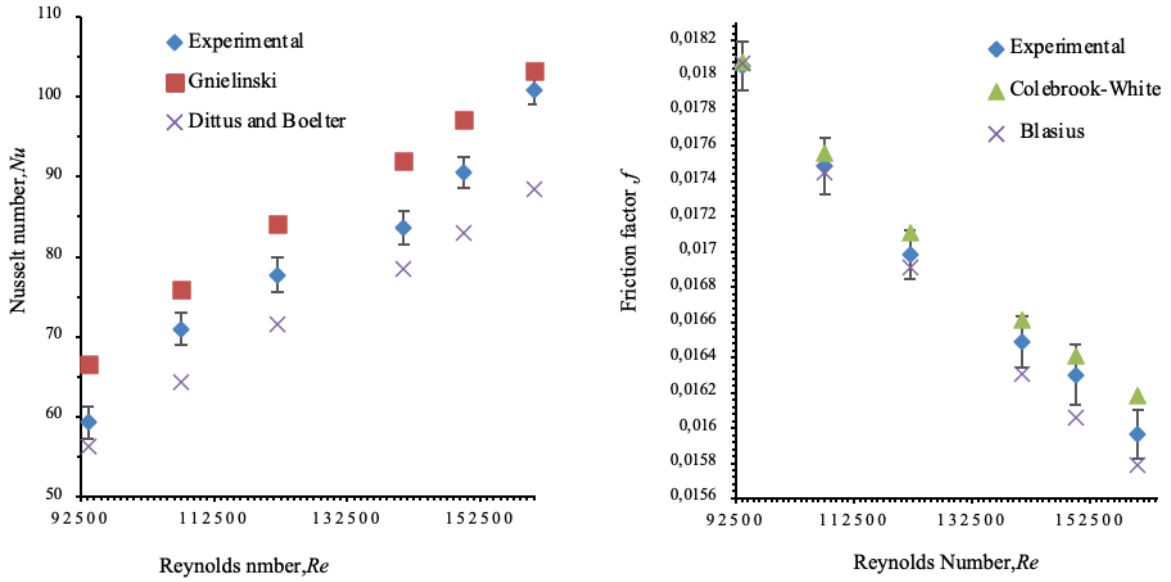

Figure 5. Assessment of average *Nu* and *f*. (a) *Nu* vs. *Re*; (b) *f* vs. *Re*.for duct without DBP.

Table 5. The average deviation from the experimental value.

Nu		*f*	
Equation used↓	**Avg. Deviance from experimental (%)**	**Equation used↓**	**Avg. Deviance from experimental (%)**
Dittus and Boelter	+8.195	Colebrook-White	-0.649
Gnielinski	-9.054	Blasius	+0.73

Figure 5 displays good agreement between experimental outcomes and those attained using correlation, certifying the precision of experimental results with an average deviation presented in Table 5.

RESULTS AND DISCUSSION

HT Augmentation

A deflector baffle substantially enhances the HT rate within the specified range of *Re* by inducing turbulent reverse flow and disrupting the thermal boundary layer, significantly improving. Figure 6 demonstrates the fluctuation in *j* with *Re*. The *j* values for CDBP rise with a rise in Re to attain a maximum value beyond which it decreases. This fashion in *j* is analogous to all the inclination angles of DBP. The j values in all CDBP models demonstrate a consistent pattern. CDBP with α of 30° exhibits the highest *j* values among different angles. Turbulent motion involves the transfer of eddy energy, which represents the energy related to random fluid movements. This chaotic motion produces numerous convective cells, facilitating faster heat transfer than laminar flow. These cells can carry substantial quantities of energy across a wide surface area.

Furthermore, generating vortices increases the effective area through which heat can be conducted between particles, thereby expediting the diffusion process. The formation of these vortices also leads to the presence of regions with contrasting pressure levels, rejuvenating the diminished energy essential for the convection process within a substance. As a result, heat transfer rates are accelerated. Ultimately, turbulent flow, characterized by a reduction in α, can significantly enhance the overall heat transfer within a medium. This flow pattern introduces considerable variability and obstruction in motion. The agitation intensifies as α decreases, culminating in heightened instability in the flow.

Additionally, there is a potential for hindrance to the development of the thermal boundary layer on the tube wall, which could reduce HT resistance. The α between the baffle plate and the deflector leads to an instant expansion of the surface area where the air comes into contact, thereby dispersing the excessive air pressure and reducing viscous losses near the tube and duct walls. Consequently, an increase in pressure loss will inevitably occur to enhance the HT rate. As presented in Figure 6, due to the sudden decline in flow passage area at baffles for smaller α, the duct side fluid velocity surges, which results in a jet effect and

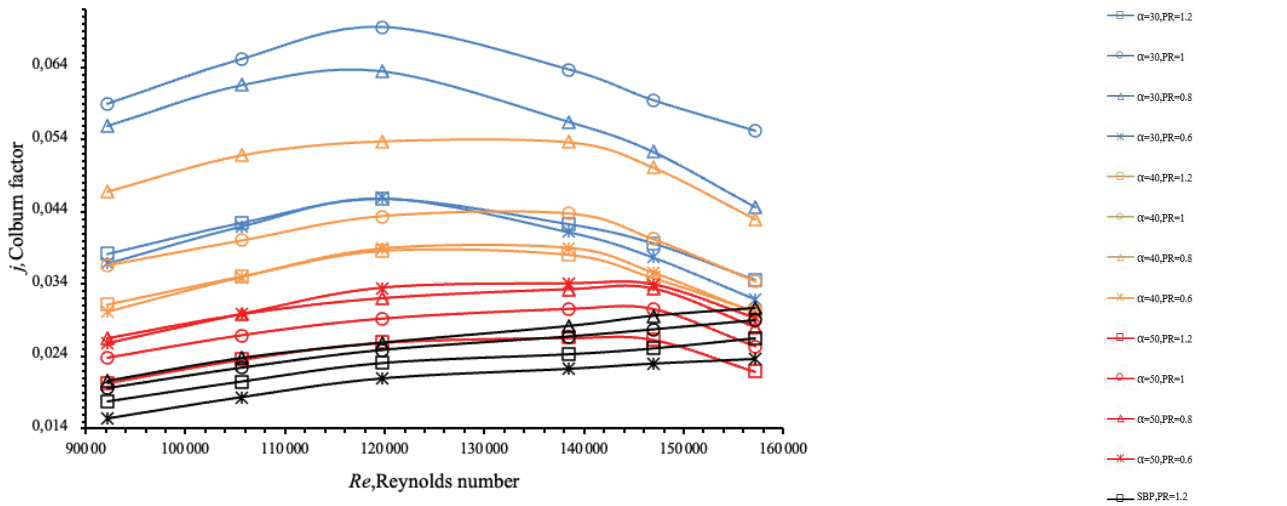

Figure 6. Effect on *j* with the variation in *Re*.

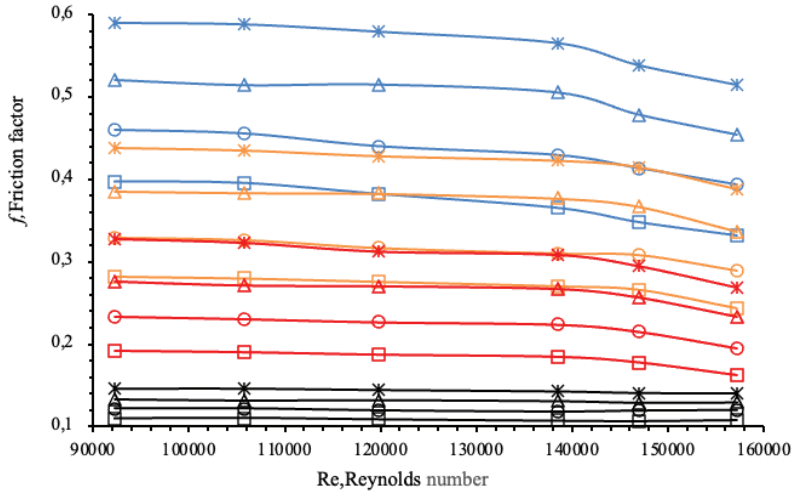

Figure 7. Effect on *f* with the change in *Re*.

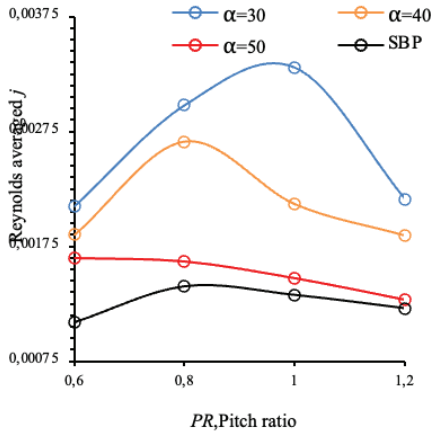

Figure 8. Reynolds averaged *j* value with *PR*.

devastation to the boundary layer formation over the tube and wall, also the fluid revolution washes the tube bundles. The spiral motion produces good mixing, directly leading to improved heat transfer. Moreover, a higher flow velocity enhances the duct-side fluid flushing ability.

The study conducted by Zhao et al. [41] showed the importance of *PR*, indicating that downstream vortex flow surges with declining down-wash spacing. On the contrary, when the spacing is excessively narrow, the contact among the vortex flows becomes intense, resulting in the breakup of vortices and a reduction in heat transfer enhancement. Conversely, wider spacings would cause an abrupt parting of the vortex flow commencing the boundary layer, prominent to undesirable high Δp. It is, therefore, crucial to determine the optimal spacing of the down-wash baffle plate (PR) to maximize HT fully.

To understand the effect of *PR*, Reynolds averaged values of *j* were plotted against *PR* for different α values. Figure 7 shows that max *j* is obtained at a lower *α* value and higher *PR* value, which explains Zhao et al.'s [41] claim regarding the secondary flow, vortex formation, and flow reattachment. As portrayed in Figure 8, inconsistency in Reynolds average (*j*) ensues with the *PR* variation. The turbulence intensity amongst the baffle plates changes with *PR*; hence HT rate will vary. Averaged *j* is higher for all α values and attains a maximum of 0.0033 at PR=1 for $\alpha=30^0$, which is 57.67 % higher than the maximum value obtained in the case of the duct with SBP.

Flow Resistance

The friction factor (*f*) value was calculated using equation 9, depicted in Figure 7, versus the Reynolds number (*Re*). All of the CDBP samples presented a similar pattern for a given range of Re, with the value of *f* being high at a low *Re* and

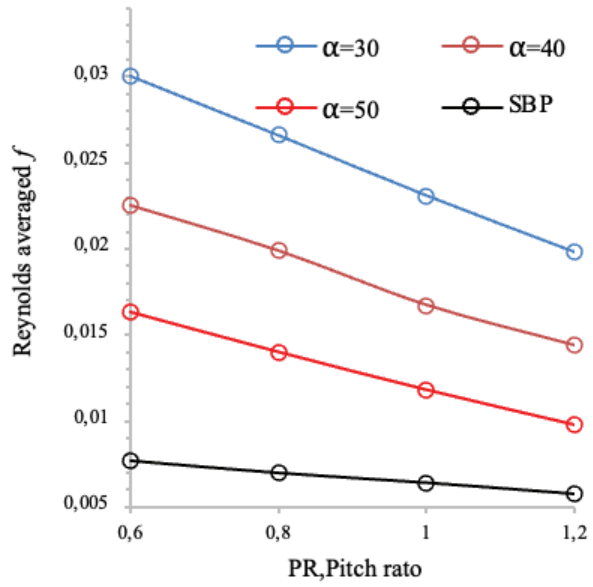

Figure 9. Reynolds averaged *f* value with *PR*.

reducing as *Re* increases. It has been found that a significant blockage of the airflow and high turbulence at an angle of 30° increases heat transfer, which in turn causes a rise in pressure drop. The pressure drops are further accentuated in areas with higher velocity, and the turbulence and contact between the surface and the fluid are higher. Therefore, it can be concluded that the order in which the pressure drops from highest to lowest would be the following: 30°, 40°, and 50°, as visible from the plot in Figure 9.

Performance Parameter

Two different parameters, such as the volume goodness factor and performance enhancement factors, are used to estimate the performance of CDBP.

The volume goodness factor is estimated as ($j/f^{1/3}$) and is seen in Figure 10, where a plot between the volume goodness factor and *Re*.

Figure 10 shows that $j/f^{1/3}$ is highest for smaller α angle and *Re* and reduces with an increase in α and *Re*, which means that at α=30 ⁰ the ratio of $j/f^{1/3}$ is higher than other α and SBP samples or, in other words, a greater convective heat transfer rate at a lower pressure drop, an essential requirement for a compact heat exchanger.

The *Re* at which the highest $j/f^{1/3}$ is obtained reduces with an increase in α. The Reynolds averaged value of $j/f^{1/3}$ seen in Figure 11 shows the highest of 0.00437 in $j/f^{1/3}$ value is obtained at higher *PR* value which reduces with increase in α. Table 6 below shows the details about the max performance values. Upon comparing CDBP with SBP, it is observed that not all α are beneficial. For a given range of *Re,* smaller α proves more efficient than larger, showing a maximum percentage rise of 38.48 % for α=30⁰ at *PR*=1 and a lower *Re*.

The thermal efficiency is shown in Figure 12, which is as high as 2.51 for α=30⁰ at PR=1.this value reduces with an increase in α; moreover, the *PR* at which max η is obtained reduces with an increase in α.

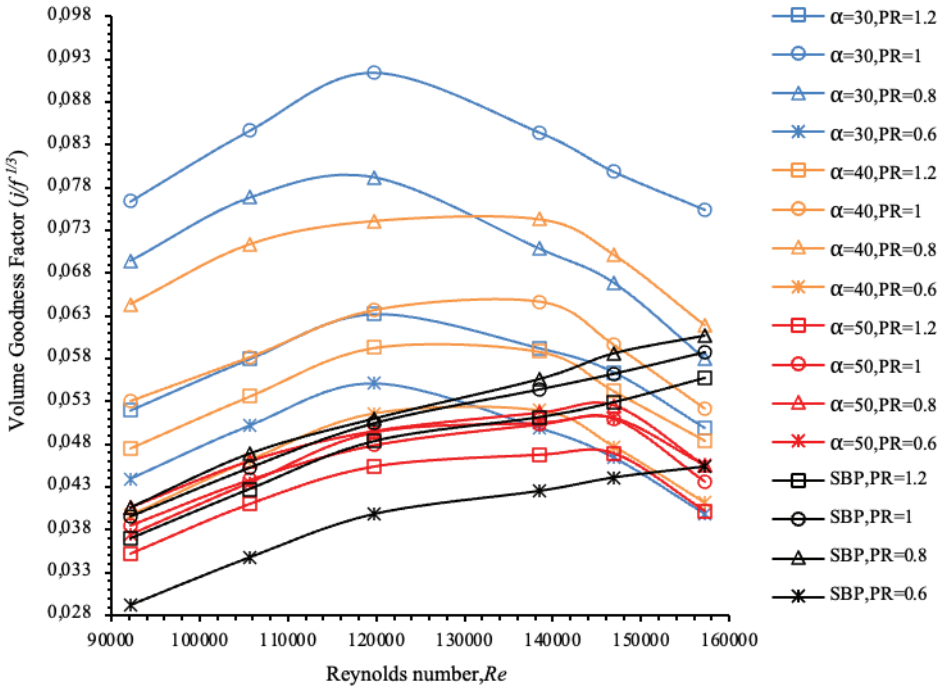

Figure 10. Volume goodness factor vs *Re*.

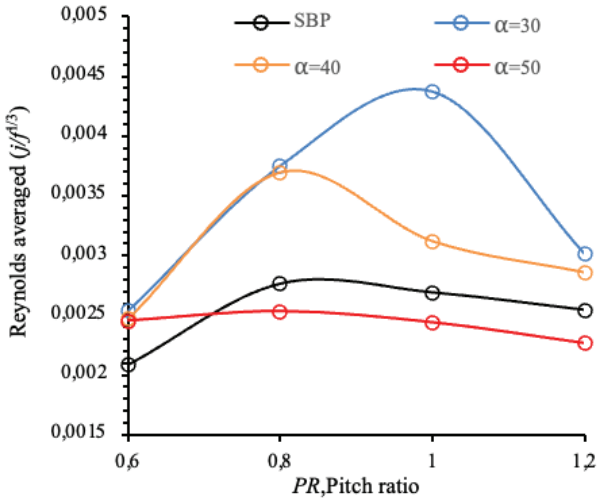

Figure 11. Reynolds avg ($j/f^{1/3}$) with *PR*.

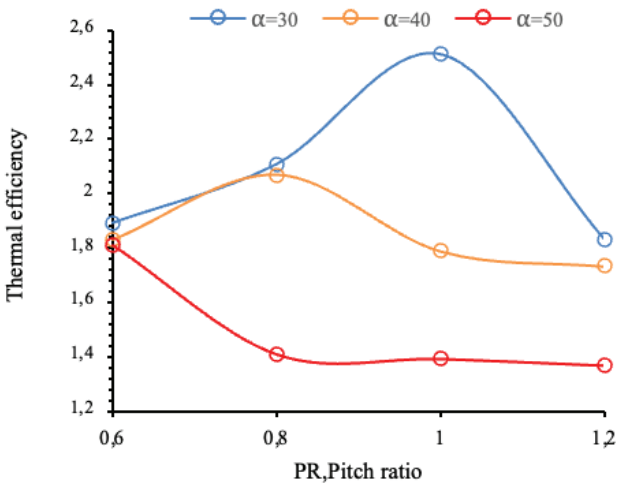

Figure 12. Thermal efficiency vs *PR*.

Table 6. The max and percentage improvement values

Inclination angle	Reynolds number	PR	$j/f^{1/3}$	Reynolds averaged $j/f^{1/3}$	Percentage Rise
α=30^0	119800	1	0.0914	0.004373	38.48
α=40^0	138500	0.8	0.0742	0.00369	27.10
α=50^0	147000	0.8	0.0525	0.002532	-6.2
SBP	157300	0.8	0.0606	0.00269	-----

CONCLUSION

A CDBP tailored in a circular test section was analyzed experimentally to compare the volume goodness factor under turbulent flow conditions. Deflector baffles caused the fluid in the duct to flow in a rotary pattern, creating a spiral movement near the tube bundle, improving the fluid flow in the axial direction, creating a plug flow, and eliminating dead zones near the baffles. The swirling motion of the fluid increased fluid mixing and HT rate but at the cost of higher Δp. The HT and Δp values depended on the *PR* and α values. Upon relating CDBP samples, it is eminent that

- ✓ For the given *Re* range, the *j* value for CDBP shows a significantly higher value for lower α, which reduces with an increase in α.
- ✓ The *PR* at which maximum (*j*) is obtained reduces with an increase in α, with the *PR* value shifting from 1 at α=30° to PR=0.6 for α=50°.
- ✓ The *Re* at which supreme *j* is obtained surges with a reduction in α
- ✓ For the given *Re* range, *f* reduces with an increase in *Re* and α further, it also reduces with an increase in *PR*
- ✓ For the given *Re* range, the $j/f^{1/3}$ value for CDBP shows a significantly higher value for lower α, which reduces with an increase in α.
- ✓ The *PR* at which maximum $j/f^{1/3}$ is obtained reduces with an increase in α, with the *PR* value shifting from 1 at α=30° to PR=0.6 for α=50°.
- ✓ The *Re* at which maximum $j/f^{1/3}$ is obtained increases with a reduction in α from 119800 at α=30° to 147000 for α=50°.
- ✓ Upon comparison of CDBP with SBP shows that lower value like 30 and 40 provides an improvement of about 25 to 40 % in Reynolds averaged $j/f^{1/3}$ values.
- ✓ Thermal efficiency is highest at lower α and higher PR value, which reduces with a rise in α.

The influence of *Pr* is on *Re* needs to investigated by changing the temperature range. The effect of tube number and orientation can be studied. Additionally, testing can be done by changing the working fluid from air to water to find its application in shell and tube HX.

NOMENCLATURE

HX	Heat exchanger
HT	Heat transfer
STHX	Shell and tube heat exchanger
CDBP	Conical deflector baffle plate
SBP	Segmental baffle plate
Nu	Nusselt number
TEF	Thermal Enhancement factor
PEC	Performance Enhancement factor

VGF	London area goodness factor
DAC	Data Acquisition system
Re	Reynolds number
PR	Pith ratio
f	Friction factor
BR	Blockage ratio
CDBP	Conical Deflector baffle plate
D	Duct inner diameter
d	Tube outer diameter
v	Average axial velocity (m/s)
Δp	Pressure drop is the test section's (Pa)
Q	Heat transfer rate for air (Watts)
A_p	Heat transfer surface area (m^2)
Δp_o	Pressure drop in orifice plate in (Pa)
Δt_{lm}	LMTD (Duct and tube wall)
α	Inclination angle
l	Distance between baffle plate (m)
A_c	Flow area (m^2)
D_e	Equivalent diameter (m)
Pr	Prandtl number of air
h_m	Avg convective heat transfer coefficient ($W/m^2.K$)
k_p	Thermal conductivity of Plexiglass (W/m·K)
k_t	Thermal conductivity of the copper tube (W/m·K)

Greek symbols

ρ	Density, kg m^{-3}
μ	coefficient of dynamic viscosity, (kg/m.s)
α	inclination angle (angle made by deflector with baffle plane)
v	average velocity, (m/s)
λ	Thermal conductivity of air
η	Thermal efficiency

Subscripts

in	Refers to the inlet
out	Refers to the outlet
w	Refers to water
a	Refers to air

AUTHORSHIP CONTRIBUTIONS

Authors equally contributed to this work.

DATA AVAILABILITY STATEMENT

The authors confirm that the data that supports the findings of this study are available within the article. Raw data that support the finding of this study are available from the corresponding author, upon reasonable request.

CONFLICT OF INTEREST

The author declared no potential conflicts of interest with respect to the research, authorship, and/or publication of this article.

ETHICS

There are no ethical issues with the publication of this manuscript.

REFERENCES

[1] Webb RL. Principles of Enhanced Heat Transfer. 2nd ed. New York: John Wiley & Sons; 1994.

[2] Choudhury R, Das UJ. Viscoelastic effects on the three-dimensional hydrodynamic flow past a vertical porous plate. Int J Heat Technol 2013;31:1−8.

[3] Ali Q, Riaz S, Memon IQ, Chandio IA, Amir M, Sarris IE, et al. Investigation of magnetized convection for second-grade nanofluids via Prabhakar differentiation. Nonlinear Engineer 2023;12:286. [CrossRef]

[4] Gupta SK, Misra RD. Flow boiling heat transfer performance of copper-alumina micro-nanostructured surfaces developed by forced convection electrodeposition technique. Chem Engineer Process 2021;164:108408. [CrossRef]

[5] Ahmadi N, Ashrafi H, Rostami S, Vatankhah R. Investigation of the effect of gradual change of the inner tube geometrical configuration on the thermal performance of the double-pipe heat exchanger. Iran J Chem Chem Engineer 2023;42:2305−2317.

[6] Gupta AK, Lilley DG, Syred N. Swirl Flows. London: Abacus Press; 1984.

[7] Thianpong C, Yongsiri K, Nanan K, Eiamsa-ard S. Thermal performance evaluation of heat exchangers fitted with twisted-rings turbulators. Int Commun Heat Mass Transf 2012;39:861−868. [CrossRef]

[8] Sheikholeslami M, Gorji-Bandpy M, Ganji DD. Review of heat transfer enhancement methods: Focus on passive methods using swirl flow devices. Renew Sustain Energy Rev 2015;49:444−469. [CrossRef]

[9] Alam HS, Redhyka GG, Bahrudin B, Sugiarto AT, Salim TI, Mardhiya IR. Design and performance of swirl flow microbubble generator. Int J Engineer Technol 2018;7:66−69.

[10] Carlos Berrio J, Pereyra E, Ratkovich N. Computational fluid dynamics modelling of gas-liquid cylindrical cyclones, geometrical analysis. ASME J Energy Resour Technol 2018;140:092003. [CrossRef]

[11] Erdal FM, Shirazi SA. Local velocity measurements and computational fluid dynamics (CFD) simulations of swirling flow in a cylindrical cyclone separator. J Energy Resour Technol 2004;126:326−333. [CrossRef]

[12] Pang X, Wang C, Yang W, Fan H, Zhong S, Zheng W, et al. Numerical simulation of a cyclone separator to recycle the active components of waste lithium batteries. Engineer Appl Comput Fluid Mech 2022;16:937−951. [CrossRef]

[13] Guillaume DW, Judge TA. Improving the efficiency of a jet pump using a swirling primary jet. Rev Sci Instrum 2004;75:553−555. [CrossRef]

[14] Zhao H, Wang F, Wang C, Chen W, Yao Z, Shi X, et al. Study on the characteristics of horn-like vortices in an axial flow pump impeller under off-design conditions. Engineer Appl Comput Fluid Mech 2021;15:1613−1628. [CrossRef]

[15] Granados-Ortiz FJ, Leon-Prieto L, Ortega-Casanova J. Computational study of the application of Al2O3 nanoparticles to forced convection of high-Reynolds swirling jets for engineering cooling processes. Engineer Appl Comput Fluid Mech 2021;15:1−22. [CrossRef]
[16] Ali Q, Amir M, Raza A, Khan U, Eldin SM, Alotaibi AM, et al. Thermal investigation into the Oldroyd-B hybrid nanofluid with the slip and Newtonian heating effect: Atangana-Baleanu fractional simulation. Front Mater 2023;10:1114665. [CrossRef]
[17] Hamzaoui MMA, Al-Khaled K, Farid S, Ali Q, Raza A, Khan SU, et al. Thermal transport of mixed convective flow of carbon nanotubes with Fourier heat flux model: Prabhakar-time derivatives assessment. Int J Mod Phys B 2023;2450057. [CrossRef]
[18] Le QH, Ali Q, Al-Khaled K, Amir M, Riaz S, Khan SU, et al. Study of hybrid nanofluid containing graphene oxide and molybdenum disulfide nanoparticles with engine oil base fluid: A non-singular fractional approach. Ain Shams Engineer J 2023;15:102317. [CrossRef]
[19] Riaz S, Ali Q, Khanam Z, Rezazadeh H, Esfandian H. Modeling and computation of nanofluid for thermo-dynamical analysis between vertical plates. Proc Inst Mech Engineer 2023;237:1750−1760. [CrossRef]
[20] Shirvan MK, Mamourian M, Esfahani AJ. Experimental investigation on thermal performance and economic analysis of cosine wave tube structure in a shell and tube heat exchanger. Energy Conver Manage 2018;175:86−98. [CrossRef]
[21] Pal E, Kumar I, Joshi JB, Maheshwari NK. CFD simulations of shell-side flow in a shell-and-tube type heat exchanger with and without baffles. Chem Engineer Sci 2016;143:314−340. [CrossRef]
[22] Abd AA, Kareem MQ, Naji SZ. Performance analysis of shell and tube heat exchanger: Parametric study. Case Stud Therm Engineer 2018;12:563−568. [CrossRef]
[23] Moharana S, Bhattacharya A, Das MK. A critical review of parameters governing the boiling characteristics of tube bundle on shell side of two-phase shell and tube heat exchangers. Therm Sci Engineer Prog 2022;29:101220. [CrossRef]
[24] Salahuddin U, Bilal M, Ejaz H. A review of the advancements made in helical baffles used in shell and tube heat exchangers. Int Comm Heat Mass Transf 2015;67:104−108. [CrossRef]
[25] Chit SP, San NA, Soe MM. Flow analysis in shell side on the effect of baffle spacing of shell and tube heat exchanger. Int J Sci Technol Soc 2015;3:254−259. [CrossRef]
[26] Bell KJ, Mueller AC. The Heat Transfer Data Book II: Fundamental Heat Transfer and Application Know-How. Lisbon: Publico Publications; 2016.
[27] Raju SN. Fluid Mechanics, Heat Transfer, and Mass Transfer Chemical Engineering Practice. 1st ed. New York: John Wiley & Sons; 2011. [CrossRef]
[28] Kongkaitpaiboon V, Nanan K, Eiamsa-ard S. Experimental investigation of heat transfer and turbulent flow friction in a tube fitted with perforated conical rings. Int Comm Heat Mass Transf 2010;37:560−567. [CrossRef]
[29] Kongkaitpaiboon V, Nanan K, Eiamsa-ard S. Experimental investigation of convective heat transfer and pressure loss in a round tube fitted with circular-ring turbulators. Int Comm Heat Mass Transf 2010;37:568−574. [CrossRef]
[30] Rahman MA, Dhiman SK. Investigations of the turbulent thermo-fluid performance in a circular heat exchanger with a novel flow deflector-type baffle plate. Bull Pol Acad Sci 2023;71:e145939. [CrossRef]
[31] Rahman MA, Dhiman SK. Performance evaluation of turbulent circular heat exchanger with a novel flow deflector-type baffle plate. J Engineer Res 2023;100105. [CrossRef]
[32] Rahman MA. Effectiveness of a tubular heat exchanger and a novel perforated rectangular flow-deflector type baffle plate with opposing orientation. World J Engineer 2023 Sept 27. doi: https://doi.org/10.1108/WJE-06-2023−0233. [Epub ahead of print]. [CrossRef]
[33] Rahman MA. Experimental investigations on single-phase heat transfer enhancement in an air-to-water heat exchanger with rectangular perforated flow deflector baffle plate. Int J Thermodyn 2023;26:31−39. [CrossRef]
[34] Coleman HW, Steele WG. Experimentation, Validation, and Uncertainty Analysis for Engineers. New York: John Wiley & Sons; 2018. [CrossRef]
[35] Cao YZ. Experimental Heat Transfer. 1st ed. Beijing: National Defence Industry Press; 1998.
[36] Hwang SW, Kim DH, Min JK. CFD analysis of fin tube heat exchanger with a pair of delta winglet vortex generators. J Mech Sci Technol 2012;26:2949−2958. [CrossRef]
[37] Dittus FW, Boelter LMK. Heat Transfer in Automobile Radiators of the Tubular Type. Publication on Engineering. 2nd ed. Berkeley: University of California Press; 1930. pp. 443−461.
[38] Gnielinski V. New equations for heat and mass transfer in turbulent pipe and channel flow. Int Chem Engineer 1976;16:359−368.
[39] White FM. Fluid Mechanics. Boston: McGraw-Hill Press; 2003.
[40] Blasius H. Das Ähnlichkeitsgesetz bei Reibungsvorgängen in Flüssigkeiten. In: Mitteilungen über Forschungsarbeiten auf dem Gebiete des Ingenieurwesens. Mitteilungen über Forschungsarbeiten auf dem Gebiete des Ingenieurwesens, vol 131. Berlin, Heidelberg: Springer; 1913. pp. 1−41. [CrossRef]
[41] Zhao H, Wang F, Wang C, Chen W, Yao Z, Shi X, et al. Study on the characteristics of horn-like vortices in an axial flow pump impeller under off-design conditions. Engineer Appl Comput Fluid Mech 2021;15:1613−1628. [CrossRef]